GASTROINTESTINAL

Potential value of CT radiomics in the distinction of intestinal-type gastric adenocarcinomas

Yue Wang[1] · Wei Liu[1] · Yang Yu[2] · Wei Han[3] · Jing-Juan Liu[1] · Hua-Dan Xue[1] · Jing Lei[1] · Zheng-Yu Jin[1] ·
Jian-Chun Yu[4] (ORCID)

Abstract

Objective The purpose of the study was to investigate the role of CT radiomics for the preoperative distinction of intestinal-type gastric adenocarcinomas.

Materials and methods A total of 187 consecutive patients with preoperative contrast CT examination and pathologically proven gastric adenocarcinoma were retrospectively collected. Patients were divided into a training set ($n = 150$) and a test set ($n = 37$). Arterial phase (AP), portal phase (PP), and delay phase (DP) images were retrieved for analysis. A dedicated postprocessing software was used to segment the lesions and extract radiomics features. Random forest (RF) algorithm was applied to construct the classifier models. A nomogram was developed by incorporating multiphase radiomics scores. Receiver operating characteristic (ROC) curves were used to evaluate the performance of the radiomics model and nomogram in both sets.

Results The radiomics model showed a favorable capability in the distinction of intestinal-type gastric adenocarcinomas. The areas under curves (AUCs) of the AP, PP, and DP radiomics models were 0.754 (95% CI: 0.676, 0.820), 0.815 (95% CI: 0.744, 0.874), and 0.764 (95% CI: 0.688, 0.829) in the training set, respectively, which were confirmed in the test set with AUCs of 0.742 (95% CI: 0.572, 0.872), 0.775 (95% CI: 0.608, 0.895), and 0.857 (95% CI: 0.703, 0.950), respectively. The nomogram yielded excellent performance for distinguishing intestinal-type adenocarcinomas in both sets, with AUCs of 0.928 (95%: 0.875, 0.964) and 0.904 (95% CI: 0.761, 0.976).

Conclusions The multiphase CT radiomics nomogram holds promise for the individual preoperative discrimination of intestinal-type gastric adenocarcinoma.

Key Points
- *CT radiomics has a potential role in the distinction of intestinal-type gastric adenocarcinomas.*
- *Single-phase enhanced CT-based radiomics showed favorable capability in distinguishing intestinal-type tumors.*
- *The nomogram which incorporates the multiphase radiomics scores could facilitate the individual prediction of intestinal-type lesions.*

Keywords Gastric cancer · Pathology · Nomogram

Abbreviations
AP	Arterial phase
AUC	Area under curve
CART	Classification and regression trees

✉ Zheng-Yu Jin
  jinzy@pumch.cn

✉ Jian-Chun Yu
  yu-jch@163.com

1 Department of Radiology, Peking Union Medical College Hospital, Chinese Academy of Medical Sciences, Peking Union Medical College, No. 1, Shuaifuyuan, Dongcheng District, Bejing 100730, People's Republic of China

2 CT Collaboration, Siemens Healthineers Ltd, 59# Beizhan Road, Shenyang 110013, People's Republic of China

3 Department of Epidemiology and Biostatistics, Institute of Basic Medical Sciences, School of Basic Medicine, Chinese Academy of Medical Sciences, Peking Union Medical College, No. 5, Dongdansantiao Street, Beijing 100005, People's Republic of China

4 Department of General Surgery, Peking Union Medical College Hospital, Chinese Academy of Medical Sciences, Peking Union Medical College, No. 1, Shuaifuyuan, Dongcheng District, Beijing 100730, People's Republic of China

CI	Confidence interval
CT	Computed tomography
DCA	Decision curve analysis
DICOM	Digital Imaging and Communications in Medicine
DP	Delay phase
HER2	Human epidermal growth factor 2
ICC	Interclass intraclass correlation coefficient
IHC	Immunohistochemistry
NAC	Neoadjuvant chemotherapy
PP	Portal phase
RF	Random forest
ROC	Receiver operative characteristics
SD	Standard deviation
VOI	Volume of interest

Introduction

Gastric cancer is the fifth most common malignant disease and ranks as the third leading cause of cancer death worldwide [1]. One of the most widely used histopathological classifications of gastric adenocarcinoma is Lauren's classification, which divides lesions into intestinal, diffuse, and mixed types [2]. Intestinal-type lesions show a definite glandular structure, sometimes with papillary or solid components. The diffuse type is composed of separated single cells or small clusters of cells that diffusely infiltrate the layers of the gastric wall. Tumors comprising non-homogenous mixtures of intestinal-type and diffuse-type features are regarded as mixed type [3]. Although Lauren's classification was introduced in 1965, it is still widely accepted and currently employed [2–4]. Tumors with different histological types have distinguished molecular features and clinical behaviors [4–8]. Patients with intestinal-type lesions have higher rates of positive human epidermal growth factor 2 (HER2) [6]. More importantly, recent studies revealed that better overall survival and progression-free survival were limited to cases of intestinal-type lesions after neoadjuvant chemotherapy (NAC) [7, 8]. Thus, accurate distinction of the intestinal-type adenocarcinomas may improve the prognostic system and facilitate more personalized treatment.

The invasive gastroscopic biopsy is routinely used for preoperative establishment of Lauren's classification. Recently, there is increasing interest in identification of valuable imaging markers to noninvasively predict the biological behavior of tumors [9]. The European Society of Radiology and Radiological Society of North America also underlined the value of imaging tools in oncology [10, 11]. Radiomics is a newly emerged technique which allows automatically extracting a large number of quantitative features from medical images using data-characterization algorithms and assessing the features to improve decision support [12–14]. The dominant advantage of radiomics is that it would uncover characteristics which are difficult to identify by human visual

examination or conventional imaging tools [15, 16]. The novel radiomics technique has exhibited excellent performance in differential diagnosis, prediction of lymph node metastasis, occult peritoneal metastasis, response to therapy, and prognosis in gastric cancer [17–22]. Thus, we hypothesized that CT radiomics might add valuable information in the distinction of histological types of gastric adenocarcinomas. The aim of the current study was to investigate whether there is a role of CT radiomics for distinguishing intestinal-type gastric adenocarcinomas, which to the best of our knowledge, has not yet been reported in any published radiological studies.

Materials and methods

Patients

The institutional review board approved the retrospective study and waived written informed consent. A total of 187 subjects (122 males and 65 females; mean age, 60.8 ± 11.7 years; age range, 22–86 years) who were treated at our institution between July 2014 and October 2018 were consecutively included. Inclusion criteria were as follows: pathologically confirmed gastric adenocarcinoma, definite Lauren's classification based on surgically gained specimens, did not receive any anticancer therapy before operation, as well as performed preoperative contrast-enhanced CT examination in our institution. The following exclusion criteria were applied: received preoperative anticancer therapy, poor image quality due to artifacts or poor distention, lack of definite information of Lauren's classification, small lesions which were difficult to locate on CT images, and linitis plastica, which can be easily established as diffuse type by the naked human eye. All eligible patients were divided into training and test sets with a ratio of 8:2 by using computer-generated random numbers [23]. Finally, 150 patients (mean age, 60.7 ± 11.9 years) were allocated into the training set and 37 patients (mean age, 61.2 ± 10.3 years) were allocated into the test set. Clinical characteristics were recorded by reviewing the electronic medical charts.

CT examination

All patients were required to fast for at least 6 h before the CT examination to empty the gastrointestinal tract and drank approximately 1000 ml water to distend the stomach prior to the examination. CT examination was performed using 64-channel (Discovery CT750, GE Medical Systems or IQon-Spectral, Philips) or dual-source CT (SOMOTOM Definition Flash, Siemens) scanners. A dose of 1.5 ml/kg of ionic contrast material (Ultravist 370, Bayer Schering Pharma) was infused to patients with a pump injector at a rate of 3.0 ml/s into the antecubital vein to acquire contrast-enhanced images.
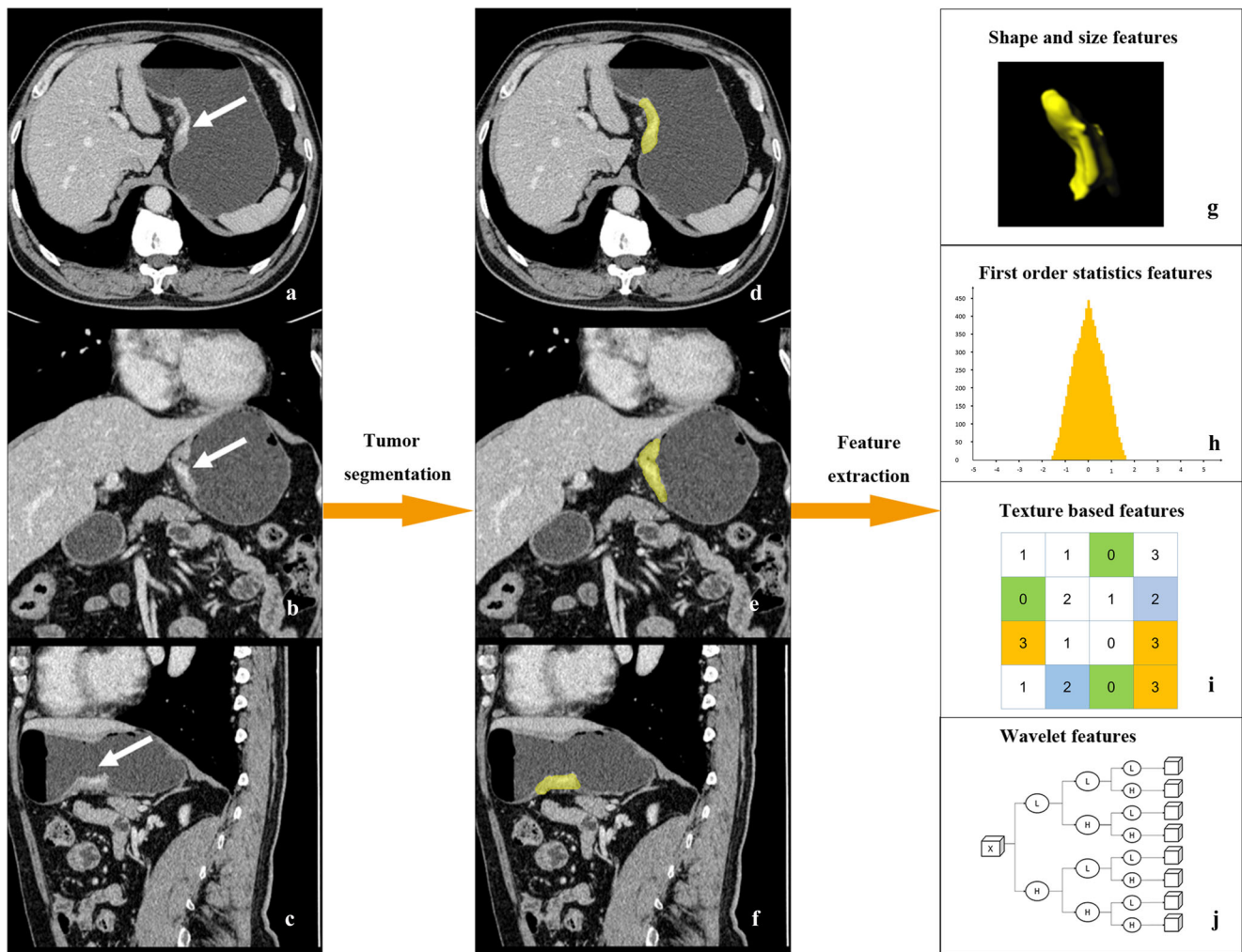
Fig. 1 An example of the tumor segmentation on PP image and subsequent feature extraction. (**a**–**c**) The tumor is detected on axial (**a**), coronal (**b**), and sagittal (**c**) PP images. (**d**–**f**) Segmentation of the entire tumor. Coronal and sagittal planes were referenced when performing the segmentation. The yellow area represents the selected region on the slice. (**g**–**j**) Extraction of four categories of radiomics features

Arterial phase (AP), portal phase (PP), and delay phase (DP) images were acquired with 25–30-s, 65–70-s, and 110–120-s delays after the injection of contrast material, respectively. The scanning, which covers the entire abdominal region, was acquired with the patient supine in all phases. The images were acquired under the tube voltage of 80 kVp for 13 patients, and 100 or 120 kVP for the rest. Other acquisition parameters were as follows: tube current, 120 to 640 mA; detector collimation of 0.625 or 0.6 mm; image matrix of 512×512; reconstruction slice thickness, 0.625 mm or 1 mm. Filtered back projection algorithm (120-kVP protocol) or advanced modeled iterative reconstruction algorithm (80-kVP protocol) was used to reconstruct images [24].

Image segmentation and feature extraction

AP, PP, and DP contrast-enhanced CT images with Digital Imaging and Communications in Medicine (DICOM) format

were retrieved for further analysis. A dedicated semi-processing "Radiomics" (syngo.via Frontier, Version 1.0.0, Siemens) prototype software was used to segment the volume of interest (VOI) and extract radiomics features. One radiologist with 6-year experience in abdominal radiology segmented the lesions of all subjects. A senior radiologist (15-year experience in abdominal radiology) segmented 35 cases (15 cases, intestinal type; 15 cases, diffuse type; 5 cases, mixed type) randomly selected from all patients to evaluate the inter-operator variability. The radiologists were blinded to clinical information and pathologic results except for the surgically proven locations of the lesions. The entire tumor was segmented, and intraluminal fluid and gas were carefully excluded. Coronal and sagittal planes were referenced when performing the segmentation. Altogether, 844 radiomics features were extracted from each VOI on each phase. The features can be divided into four categories: 16 shape and size features that describe the three-dimensional geometric

Table 1 Clinical characteristics in the training and test sets

Clinical characteristics		Training set ($n = 150$)	Test set ($n = 37$)	p value
Pathologic Lauren type, n (%)	Intestinal type	65 (43.3)	15 (40.5)	0.844
	Mixed type	30 (20)	9 (24.4)	
	Diffuse type	55 (36.7)	13 (35.1)	
Age (y), mean ± SD		60.7 ± 11.9	61.2 ± 10.3	0.786
Sex, n (%)	Female	54 (36)	11 (29.7)	0.474
	Male	96 (64)	26 (70.3)	
Tumor location, n (%)	Fundus	18 (12)	5 (13.5)	0.080
	Body	36 (24)	14 (37.8)	
	Antrum	96 (64)	18 (48.7)	
Tumor morphology, n (%)	flat	123 (82)	31 (83.8)	0.799
	Ulceration	27 (18)	6 (16.2)	
Pattern of enhancement, n (%)	homogeneous	89 (59.3)	19 (51.4)	0.380
	heterogeneous	61 (40.7)	18 (48.6)	

Data in parenthesis are percentages. Patients' age between the two sets were analyzed with t test. The other variables between the two sets were analyzed with Chi-square test.

SD, standard deviation

character of the tumor lesion; 18 first-order statistics features that demonstrate the distribution of voxel-based CT intensities within the image through common metrics; 74 texture features that indicate the relative position of the various gray levels over the image; and 736 wavelet features that were derived from a wavelet transformation of the first-order statistics and texture features. An example of tumor segmentation on PP image and subsequent feature extraction is shown in Fig. 1.

Construction of radiomics model

Radiomics models were built with our in-house software programmed with the Python Scikit-learn package (Python version 3.7, Scikit-learn version 0.21, http://scikit-learn.org/). A random forest (RF) method was used for classification of the lesions. Features with intraclass correlation coefficient (ICC) value higher than 0.8 were considered reliable and selected for subsequent analysis. Further feature selection was skipped as it helped increasing efficiency more than improving the accuracy of the model when utilizing the RF algorithm [25]. Five general features (scanning kilo-voltage, tube current, voxel number, patient age and sex) were also included for model construction to take into consideration of the scanning parameters and patient variance. RF algorithm is an ensemble learning method that constructs a number of decision trees from the randomly selected subsets of the training set

Table 2 Selected stable features on each phase and comparison of radiomics scores in patients with intestinal- and diffuse-/mixed-type lesions

Parameters	AP	PP	DP
No. of selected stable radiomics features	141	134	145
Shape and size features	7	5	6
First-order statistics	13	14	13
Texture-based features	43	44	37
Wavelet features	78	71	89
Radiomics scores in training set			
Intestinal type	0.539 ± 0.154	0.524 ± 0.149	0.547 ± 0.162
Diffuse or mixed type	0.398 ± 0.139	0.326 ± 0.160	0.361 ± 0.190
ρ value	< 0.001	0.001	< 0.001
Radiomics scores in test set			
Intestinal type	0.528 ± 0.146	0.43 ± 0.161	0.627 ± 0.114
Diffuse or mixed type	0.412 ± 0.118	0.286 ± 0.120	0.348 ± 0.192
ρ value	0.012	0.003	< 0.001

Features with ICC > 0.8 were indicated as stable

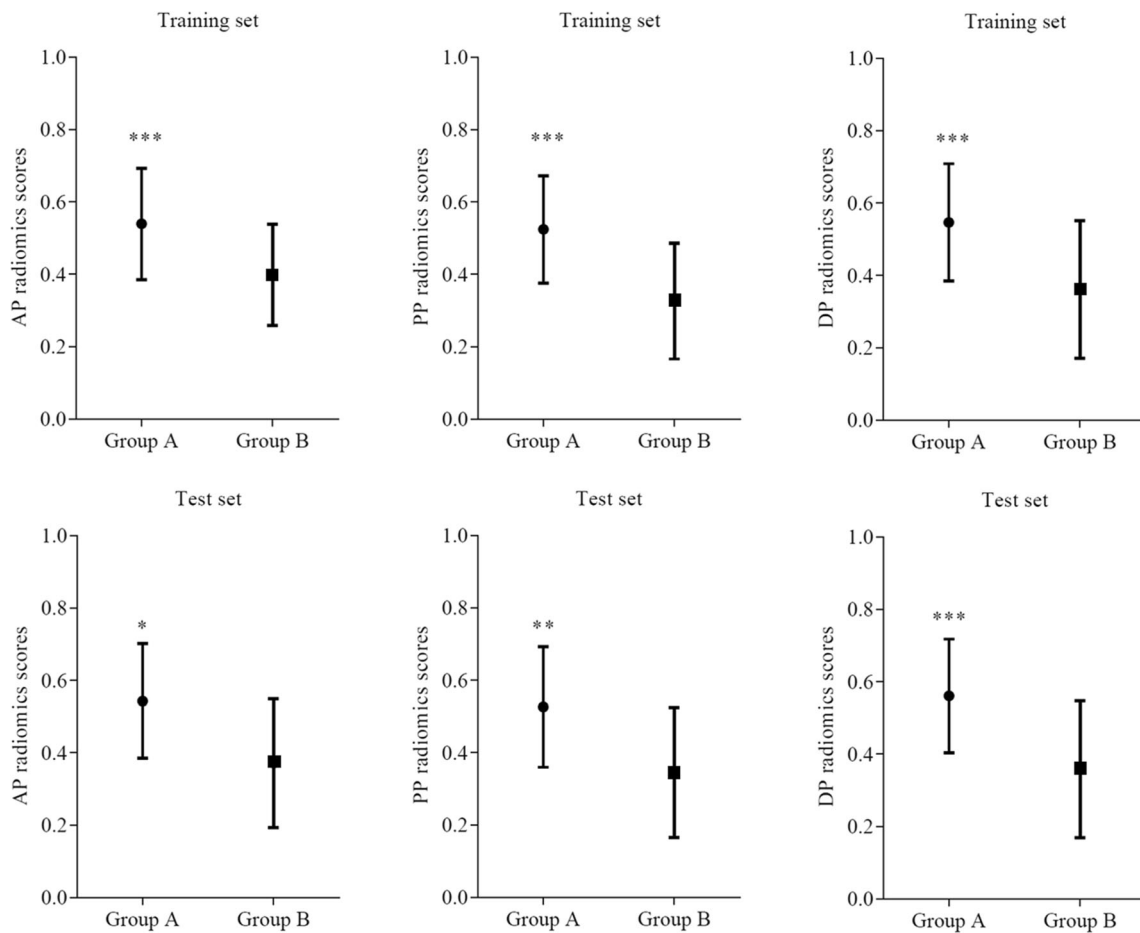*AP*, arterial phase; *PP*, portal phase; *DP*, delay phase

Fig. 2 Mean values with error bars for AP-, PP-, and DP-based radiomics scores in patients with intestinal-type and non-intestinal-type lesions. Group A: patients with intestinal-type lesions. Group B: patients with diffuse- or mixed-type lesions. The centers represent the mean values, and the bars denote SD. ***$p < 0.001$; **$p < 0.01$; *$p < 0.05$

[26]. Each classification and regression tree (CART) was established by randomly drawing bootstrap samples and features. Final prediction would be made with the bagging method by voting or averaging. Gini impurity was used for splitting the branches. Parameters such as the number of trees in the forest and the minimum sample limitation for leaf node
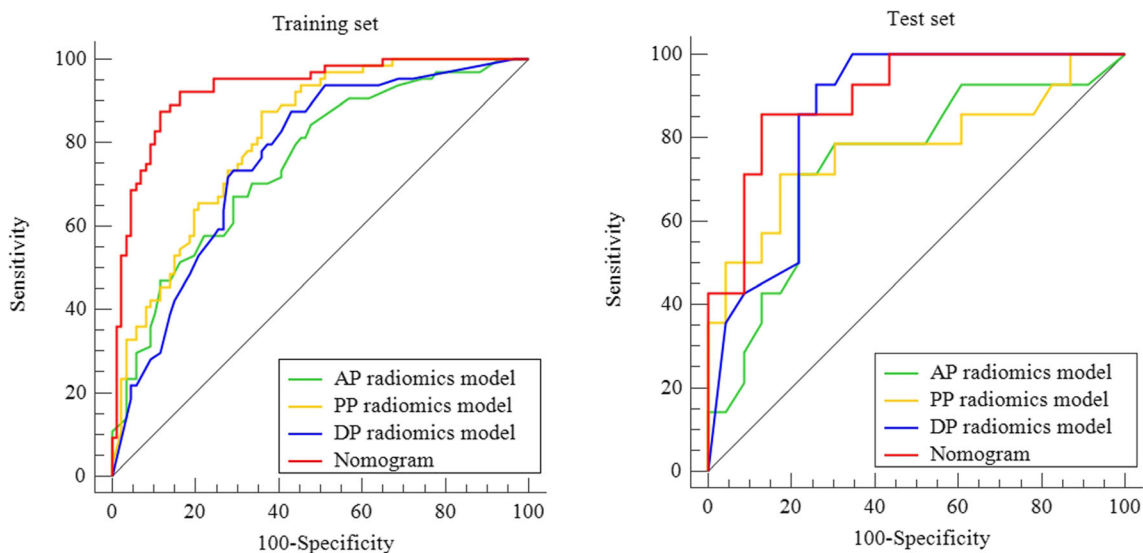
Fig. 3 ROC curves of multiphase radiomics models and nomogram in the training and test sets

Table 3 Univariate and multivariate regression analysis of clinical characteristics and multiphase radiomics scores in training set

Characteristics	Univariate analysis			Multivariate analysis		
	Odds ratio	95% CI	*p* value	Odds ratio	95% CI	*p* value
Age	0.988	(0.961, 1.016)	0.389	-	-	-
Sex	1.695	(0.852, 3.369)	0.129	-	-	-
Tumor location	0.622	(0.226, 1.714)	0.313	-	-	-
Tumor morphology	1.825	(0.788, 4.228)	0.158	-	-	-
Pattern of enhancement	0.851	(0.440, 1.645)	0.630	-	-	-
AP-Radiomics scores	519.9	(43.4, 6226.3)	< 0.001	777.9	(22.6, 26760.9)	< 0.001
PP-Radiomics scores	2642.0	(172.6, 40461.2)	< 0.001	8598.2	(257.5, 287050.0)	< 0.001
DP-Radiomics scores	238.4	(30.2, 1893.2)	< 0.001	1510.8	(68.2, 33444.5)	< 0.001

Features with ICC > 0.8 were indicated as stable

AP, arterial phase, *PP*, portal phase, *DP*, delay phase

were optimized through a 5-fold cross-validation [23]. The RF model was only trained in the training set. The best model was selected and used to predict the radiomics score in the test set. The calculated (in training set) or predicted (test set) radiomics score of each patient was recorded. Radiomics score is defined as the prediction probability of an input sample which was computed as the mean predicted class probabilities of the trees in the forest. The class probability of a single tree is the fraction of samples of the same class in a leaf [26]. The RF algorithm was applied to features extracted from AP, PP, and DP images to construct the classifier models, respectively.

Statistical analysis

The continuous variables were tested for normality by using the Kolmogorov–Smirnov test. Differences between normally distributed variables were compared with *t* test. Differences between qualitative variables were compared with Chi-square test. Inter-operator variability of the radiomics features was assessed with ICC. All available clinical variables including age, sex, location of tumor, tumor morphology, and pattern of enhancement as well as multiphase radiomics scores in the training set were evaluated with univariate and multivariate logistic regression analyses. In multivariate analysis, likelihood ratio test based on the maximum partial likelihood estimates was utilized to select the independent predictors. A quantitative nomogram was built incorporating the selected independent predictors to facilitate clinical use for prediction of intestinal type lesions. The performance of the radiomics model or nomogram in both sets was tested with receiver operator characteristics (ROC) curves based on the radiomics score or individual nomogram score, respectively. The area under curve (AUC) and 95% confidence interval (CI) were calculated [19]. The ROCs of the radiomics model between the two sets were compared with the DeLong test to evaluate whether overfitting occurred. The calibration of the

nomogram in both sets was assessed using calibration curves and Hosmer-Lemeshow test. Decision curve analysis (DCA) was conducted to evaluate the clinical usefulness of the nomogram by calculating the net benefits at different threshold probabilities. Put simply, net benefit equals the net true positives divided by the sample size [27]. Statistical analysis was analyzed with SPSS software (Version 19) and R software package (version 3.5.2: http://www.Rproject.org).

Results

Clinical characteristics

Intestinal-type, mixed-type, and diffuse-type adenocarcinomas were identified in 80, 39, and 68 patients, respectively. Table 1 summarized the clinical characteristics in training and test sets. No significant differences were found between the training and test sets regarding any clinical characteristics including the distribution of Lauren type, age, sex, tumor location, tumor morphology, or pattern of enhancement. Additionally, HER2 status by immunohistochemistry (IHC) was available for 143 out of the 187 patients. IHC3+, 2+, 1+, and 0 were found in 15, 19, 58, and 51 patients, respectively. None of the 19 patients with IHC 2+ received further fluorescence in situ hybridization test. About 86.7% (13/15) cases with positive (IHC3+) and 52.6% (10/19) cases with borderline (IHC 2+) HER2 showed intestinal-type lesions.

Construction and performance of radiomics model

There were 141, 134, and 145 reliable features selected from AP, PP, and DP images, respectively. Details of the selected stable features on each phase and comparison of radiomics scores in patients with intestinal- and diffuse-/mixed-type lesions are summarized in Table 2. Significant differences were
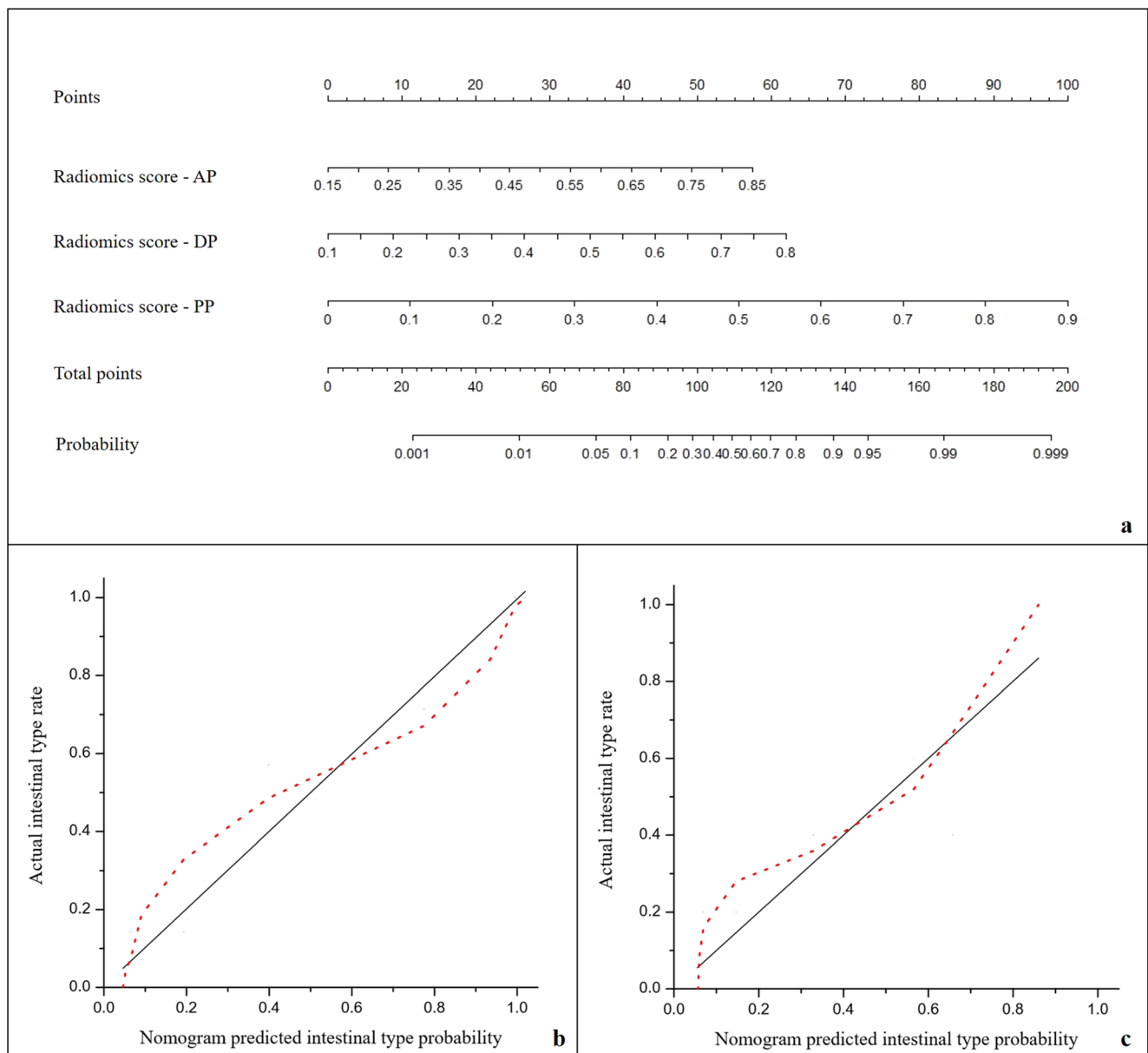
Fig. 4 a Nomogram based on the multiphase radiomics scores for the distinction of intestinal-type lesions in patients with gastric adenocarcinoma. b, c Calibration curves of the nomogram in the training set (b) and test set (c). The 45° solid line represents the perfect prediction. The dotted red line represents the predictive performance of the nomogram. The dotted line has a close fit with the solid line, which suggests good predictive capability of the nomogram

identified in radiomics scores from each phase between patients with intestinal-type and diffuse-/mixed-type lesions in both sets (Fig. 2). The radiomics models showed favorable capability in the distinction of intestinal-type gastric adenocarcinoma (Fig. 3). The AUCs of the AP, PP, and DP radiomics models were 0.754 (95% CI: 0.676, 0.820), 0.815 (95% CI: 0.744, 0.874), and 0.764 (95% CI: 0.688, 0.829) in the training set, respectively, which were confirmed in the test set with AUCs of 0.742 (95% CI: 0.572, 0.872), 0.775 (95% CI: 0.608, 0.895), and 0.857 (95% CI: 0.703, 0.950), respectively. No significant differences in ROCs between the two sets were found in any model (DeLong test: AP, $p = 0.9098$; PP, $p = 0.6752$; DP, $p = 0.1988$).

Development and clinical usefulness of radiomics nomogram

None of clinical variables showed significant p values in either univariate or multivariate analysis. All multiphase radiomics scores showed $p < 0.001$ in both the univariate and multivariate analyses. Details of the univariate and multivariate analyses were presented in Table 3. A
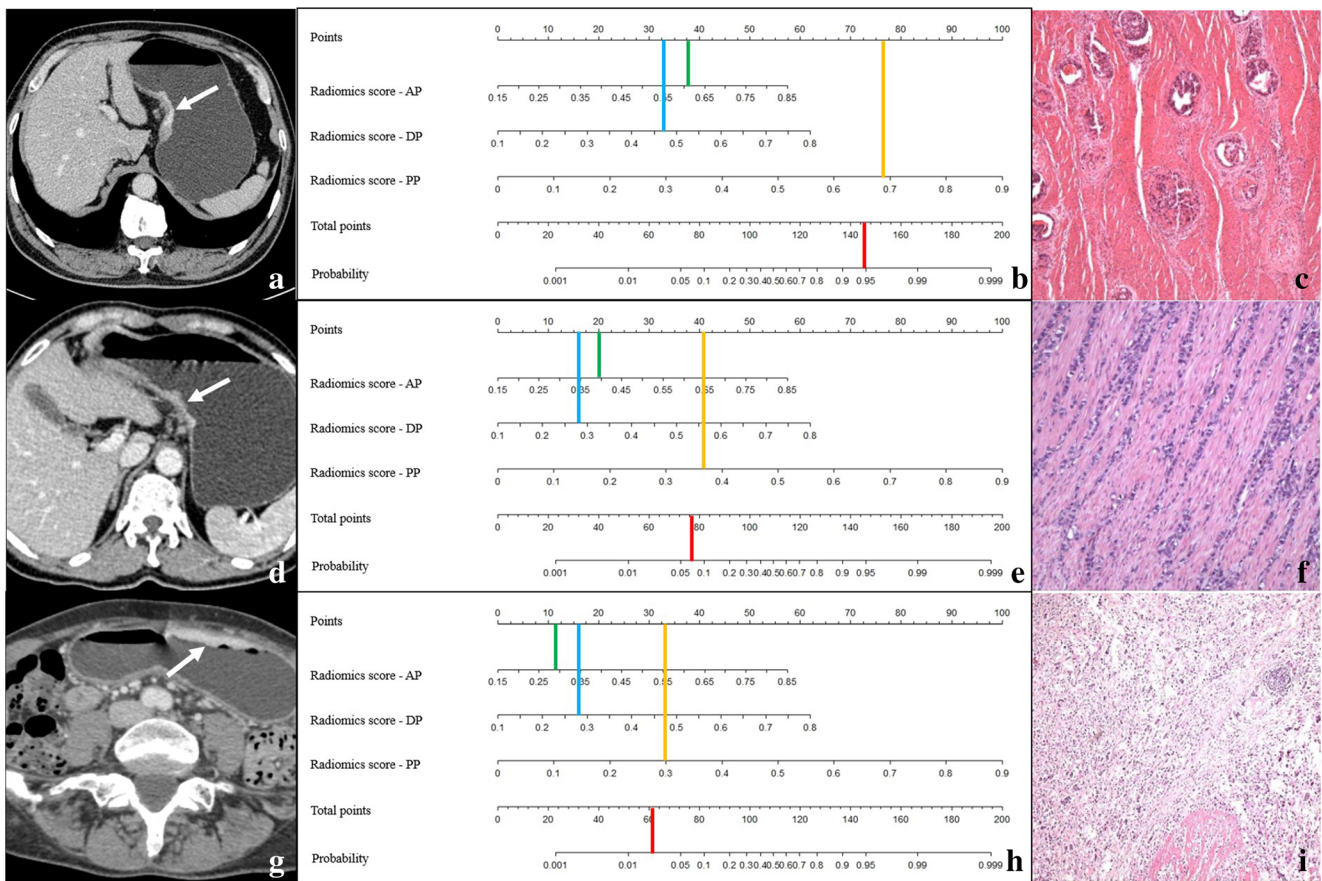
Fig. 5 Examples of using the nomogram for individual prediction of the probability of intestinal-type adenocarcinoma by simply drawing several lines: First, draw vertical lines for every variable of the patients (Radiomics score-AP, green lines; Radiomics score-PP, yellow lines; Radiomics score-DP, blue lines). Then, sum up the values intersected by the lines on the "Points" scale to obtain total points. Lastly, draw a vertical line (the red lines on **b**, **e**, and **h**) on the "Total points" scale to read the "Probability" of being intestinal-type carcinoma. (**a**–**c**) CT image (**a**) and nomogram (**b**) and microscopic pathological images (**c**, HE staining, × 10) of a 66-year-old male. A thickened lesion (**a**, white arrow) was observed in the less curvature of the stomach. The AP, PP, and DP radiomics scores were 0.61, 0.69, and 0.47 respectively. Vertical lines of each variable were drawn. The values on the "Points" scale intersected by the lines were added to get "Total points" (37 + 76 + 33 = 146). The nomogram revealed that the probability of intestinal-type tumor was 95% by drawing a vertical line on the "Total points" scale (**b**). Microscopic pathological image of the surgical specimen (**c**) proved the intestinal type. (**d**–**f**) CT image (**d**), and nomogram (**e**) and microscopic pathological images (**f**, HE staining, × 4) of a 61-year-old male. The tumor (**d**, white arrow) in the less curvature of the stomach was identified. The multiphase radiomics scores were 0.40 (AP), 0.37 (PP), and 0.28 (DP), respectively. "Total points" (20 + 41 + 16 = 77) were obtained by calculating the sum of the values on "Points" scale intersected by the lines of each variable. The nomogram displayed that the possibility of intestinal type was 7% (**e**). Postoperative microscopic pathology (**f**) found that the tumor was mixed-type adenocarcinoma. (**g**–**i**) CT image (**g**) and nomogram (**h**) and microscopic pathological image (**i**, HE staining, × 4) of a 58-year-old female with gastric cancer. A lesion in the greater curvature was detected (**g**, white arrow). The AP, PP, and DP radiomics scores were 0.29, 0.30, and 0.28, respectively. "Total points" (12 + 33 + 16 = 61) were calculated by adding the values on "Points" scale intersected by the lines. The nomogram showed that the probability of intestinal type was only 3% by drawing a vertical line on the "Total Points" scale (**h**). Microscopic pathological image (**i**) by surgical specimen revealed that the tumor was diffuse type

nomogram was built incorporating multiphase radiomics scores based on the multivariate logistic regression analysis (Fig. 4 a). The Hosmer-Lemeshow test exhibited non-significant p values of 0.732 in the training set and 0.516 in the test set suggesting that the nomogram was acceptable. The calibration curves in the training and test sets were presented in Fig. 4 b and c. The nomogram exhibited excellent performance in distinguishing intestinal-type adenocarcinoma, with AUCs of 0.928 (95% CI: 0.875, 0.964) in the training set and 0.904 (95% CI: 0.761,

0.976) in the test set (Fig. 3). Examples of using the nomogram for individual prediction of the probability of them being intestinal-type tumor are displayed in Fig. 5. Furthermore, DCA showed that when the predicted probability of being intestinal-type lesion was over 15%, the nomogram would offer more net benefits than either the default all-NAC (all patients were intestinal types) or none-NAC (no patients were intestinal types) scheme in the training cohort. DCA in the test set rendered similar results (Fig. 6).
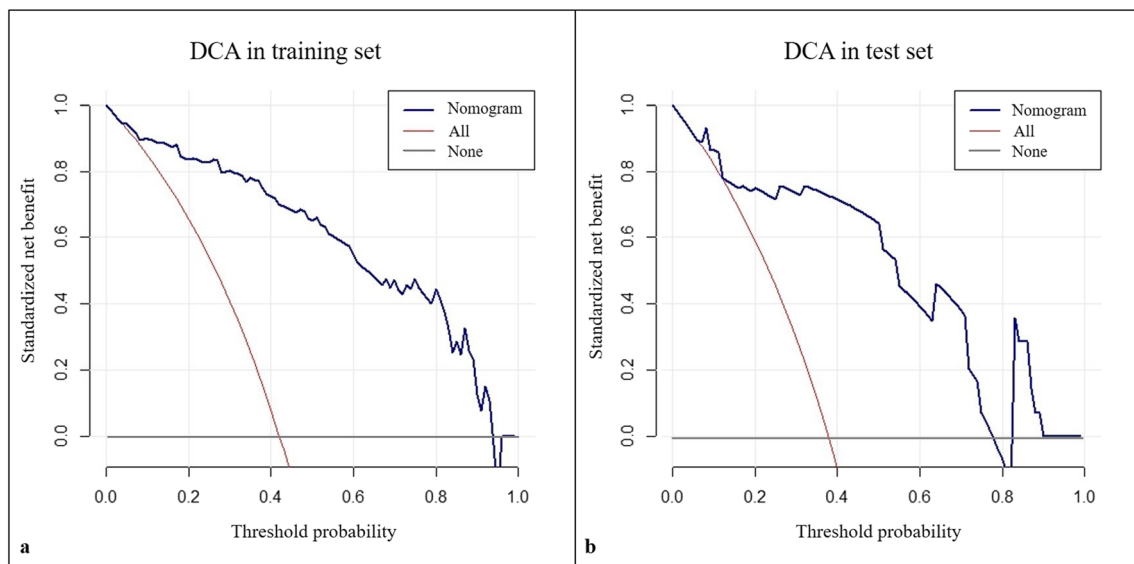
Fig. 6 DCA for the nomogram in training (**a**) and test (**b**) sets. The net benefits versus the threshold probability are plotted. The x-axis represents the predicted threshold probability. The y-axis represents the net benefit. The gray line represents the assumption that no patients have intestinal-type lesions and without NAC therapy. The red curve represents the assumption that all patients were intestinal-type lesions and receive NAC strategy. The blue curve represents the nomogram. A model is only clinically useful if it has higher net benefits than the default "all-NAC" or "none-NAC" scheme. It is obvious from the diagram that the nomogram can offer more net benefits than the default schemes across the majority of the range of threshold probabilities in both sets

Discussion

Distinction of intestinal-type gastric adenocarcinoma carries great clinical significance. This study investigated the value of CT radiomics in the discrimination of intestinal-type gastric adenocarcinomas for the first time. The key finding was that CT-based radiomics may offer potential value for the distinction of intestinal-type gastric adenocarcinomas. Furthermore, the nomogram based on the multiphase radiomics scores exhibited excellent performance for individualized prediction of intestinal-type lesions.

Tumors with disparate Lauren type have distinguished molecular characteristics. Previous studies suggested that HER2 positivity rate is higher in the intestinal-type adenocarcinoma [28]. This study showed similar results with 86.7% HER2-positive patients showing intestinal-type lesions. What's more, prognosis of NAC therapy varies significantly between patients with different Lauren types; better patient outcomes were found only in patients with intestinal-type adenocarcinomas [7, 8]. In these circumstances, accurate distinguishing of the intestinal-type lesions may benefit patients by promoting the prognostic system and optimizing management strategy. Preoperative evaluation of the Lauren classification conventionally relies on invasive gastroscope biopsy in routine practice, while the role of biopsy may be restricted when the specimens are taken from partially heterogeneous tumors. The documented accuracy of biopsy was unsatisfactory in the earlier studies, especially in distinguishing intestinal-type lesions. Approximately 21–27% biopsy-suggested intestinal-type carcinomas were proved to be mixed or diffuse types [29, 30].

Although researches evaluating the capability of biopsy for diagnosis of Lauren type were rare lately, the accuracy would definitely be much higher with the booming of technology. Be that as it may, any imaging-guided wise thought is always beneficial and valuable in planning disease management [9]. Prior studies have evaluated the association between CT or MRI parameters and Lauren classification. In the work conducted by Liu et al [31], several CT texture features including all percentiles and modes derived from PP CT images ($r = 0.228$–0.321) as well as standard deviation and entropy derived from AP CT images ($r = -0.222$) were found to be correlated with Lauren classification. Another study carried out by Liu S et al [32] found that mean ($r = -0.493$) and minimum ($r = -0.481$) apparent diffusion coefficients were correlated with Lauren classification. Ma et al [33] reported that extracellular extravascular volume fraction—one of the dynamic contrast MRI parameters—was significantly differed between intestinal- and diffuse-type lesions. This study investigated the value of CT radiomics for distinction of intestinal-type lesions. The single-phase CT radiomics models in this study showed favorable capability for distinction of intestinal-type from diffuse- or mixed-type gastric adenocarcinomas, with AUC values ranging from 0.754 to 0.815 in the training set and from 0.742 to 0.857 in the test set. The results substantiate that the radiomics approach may add potential value in enhancing image interpretations and facilitating preoperative distinction of intestinal-type adenocarcinomas.

Another pearl of this study was the construction of the easy-to-use nomogram based on the multiphase radiomics scores for clinical individual prediction of the probability of

intestinal-type lesions. Nomogram is a graphical calculating device which enables approximate computation by simply drawing several lines. The radiomics-based nomogram in the current study yielded excellent performance with AUCs of 0.928 and 0.904 in the training and test sets for distinction of intestinal-type lesions, respectively. Although NAC was widely recommended for locally advanced gastric cancer, better overall survival and progression-free survival were limited to cases with intestinal-type lesions after NAC therapy [7, 8]. A major problem for those who do not benefit from the NAC therapy may be the delay of the alteration of management strategy. The nomogram holds the potential to assist in optimizing the selection of appropriate candidates for NAC. DCA revealed that the current nomogram could offer net benefits over the "all-NAC" or "none-NAC" strategy across the majority of the range of threshold probabilities in both the training and test sets.

The study had several limitations. First, this was a single-center analysis; external validation in a larger cohort is necessary to confirm the performance of the radiomics nomogram. Second, the results of Lauren classifications by gastroscopic biopsy were not available for all patients due to the retrospective design of the study. Comparison of the discrepancy between the biopsy and definitive result was absent. The performance of the radiomics model and biopsy was not compared either. Third, the study mainly focused on the distinction of intestinal-type lesions from other types, and differentiation between mixed and diffuse types was not performed. Finally, the radiomics features in the current study were extracted from entire tumors; exploration of radiomics models based on more time-efficient region-based features merits further study.

In a nutshell, the study showed that the CT radiomics nomogram offers great potential in the preoperative individualized distinction of intestinal-type gastric adenocarcinomas.

Compliance with ethical standards

References

1. Bray F, Ferlay J, Soerjomataram I, Siegel RL, Torre LA, Jemal A (2018) Global Cancer Statistics 2018: GLOBOCAN estimates of incidence and mortality worldwide for 36 cancers in 185 countries. CA Cancer J Clin 0:1–31
2. Lauren P (1965) The two histological main type of gastric carcinoma: diffuse and so-called intestinal-type carcinoma. An attempt at a histo-clinical classification. Acta Pathol Microbiol Scand 64:31–49
3. Roy P, Piard F, Dusserre-Guion L, Martin L, Michiels-Marzais D, Faivre J (1998) Prognostic comparison of the pathological classifications of gastric cancer: a population-based study. Histopathology 33:304–310
4. Smyth EC, Verheij M, Allum W, Cunningham D, Cervantes A, Arnold D (2016) Gastric cancer: ESMO clinical practice guidelines for diagnosis, treatment and follow-up. Ann Oncol 27:v38–v49
5. Qiu MZ, Cai MY, Zhang DS et al (2013) Clinicopathological characteristics and prognostic analysis of Lauren classification in gastric adenocarcinoma in China. J Transl Med 11:58. https://doi.org/10.1186/1479-5876-11-58
6. Matsusaka S, Nashimoto A, Nishikawa K et al (2016) Clinicopathological factors associated with HER2 status in gastric cancer: results from a prospective multicenter observational cohort study in a Japanese population (JFMC44-1101). Gastric Cancer 19:839–851
7. Jimenez Fonseca P, Carmona-Bayonas A, Hernandez R et al (2017) Lauren subtypes of advanced gastric cancer influence survival and response to chemotherapy: real-world data from the AGAMENON National Cancer Registry. Br J Cancer 117:775–782
8. Hu SB, Liu CH, Wang X et al (2019) Pathological evaluation of neoadjuvant chemotherapy in advanced gastric cancer. World J Surg Oncol 17:3
9. Giganti F, Tang L, Baba H (2018) Gastric cancer and imaging biomarkers: part 1 - a critical review of DW-MRI and CE-MDCT findings. Eur Radiol 29:1743–1753
10. European Society of Radiology (ESR) (2010) White paper on imaging biomarkers. Insights Imaging 1:42–45
11. Buckler AJ, Bresolin L, Dunnick NR, Sullivan DC, Group (2011) A collaborative enterprise for multi-stakeholder participation in the advancement ofquantitative imaging. Radiology 258(3):906–914
12. Lambin P, Rios-Velazquez E, Leijenaar R et al (2012) Radiomics: extracting more information from medical images using advanced feature analysis. Eur J Cancer 48:441–446
13. Lambin P, Leijenaar RTH, Deist TM et al (2017) Radiomics: the bridge between medical imaging and personalized medicine. Nat Rev Clin Oncol 14:749–762

14. Kumar V, Gu Y, Basu S et al (2012) Radiomics: the process and the challenges. Magn Reson Imaging 30:1234–1248

15. Aerts HJ, Velazquez ER, Leijenaar RT et al (2014) Decoding tumour phenotype by noninvasive imaging using a quantitative radiomics approach. Nat Commun 5:4006. https://doi.org/10.1038/ncomms5006

16. Aerts HJ (2016) The potential of radiomic-based phenotyping in precision medicine: a review. JAMA Oncol 2:1636–1642

17. Ba-Ssalamah A, Muin D, Schernthaner R et al (2013) Texture-based classification of different gastric tumors at contrast-enhanced CT. Eur J Radiol 82:e537–e543

18. Mazzei MA, Nardone V, Di Giacomo L et al (2018) The role of delta radiomics in gastric cancer. Quant Imaging Med Surg 8:719–721

19. Dong D, Tang L, Li ZY et al (2019) Development and validation of an individualized nomogram to identify occult peritoneal metastasis in patients with advanced gastric cancer. Ann Oncol 30:431–438

20. Feng QX, Liu C, Qi L et al (2019) An intelligent clinical decision support system for preoperative prediction of lymph node metastasis in gastric cancer. J Am Coll Radiol 16:952–960

21. Li W, Zhang L, Tian C et al (2018) Prognostic value of computed tomography radiomics features in patients with gastric cancer following curative resection. Eur Radiol 29:3079–3089

22. Jiang Y, Chen C, Xie J et al (2018) Radiomics signature of computed tomography imaging for prediction of survival and chemotherapeutic benefits in gastric cancer. EBioMedicine 36:171–182

23. Suthaharan S (2016) Machine learning models and algorithms for big data classification: thinking with examples for effective learning, 1st edn. Springer US, New York

24. Buls N, Van Gompel G, Van Cauteren T et al (2015) Contrast agent and radiation dose reduction in abdominal CT by a combination of low tube voltage and advanced image reconstruction algorithms. Eur Radiol 25:1023–1031

25. Zani S, Riani M, Vichi M (2006) Data analysis, classification and the forward search, 1st edn. Springer, Berlin Heidelberg

26. Svetnik V, Liaw A, Tong C, Culberson JC, Sheridan RP, Feuston BP (2003) Random forest: a classification and regression tool for compound classification and QSAR modeling. J Chem Inf Comput Sci 43:1947–1958

27. Van Calster B, Wynants L, Verbeek JFM et al (2018) Reporting and interpreting decision curve analysis: a guide for investigators. Eur Urol 74:796–804

28. Qiu MZ, Li Q, Wang ZQ et al (2014) HER2-positive patients receiving trastuzumab treatment have a comparable prognosis with HER2-negative advanced gastric cancer patients: a prospective cohort observation. Int J Cancer 134:2468–2477

29. Flucke U, Monig SP, Baldus SE et al (2002) Differences between biopsy- or specimen-related Lauren and World Health Organization classification in gastric cancer. World J Surg 26:137–140

30. Qiu MZ, Shi SM, Chen M et al (2017) Comparison of HER2 and Lauren classification between biopsy and surgical resection samples, primary and metastatic samples of gastric cancer. J Cancer 8:3531–3537

31. Liu S, Liu S, Ji C et al (2017) Application of CT texture analysis in predicting histopathological characteristics of gastric cancers. Eur Radiol 27:4951–4959

32. Liu S, Guan W, Wang H et al (2014) Apparent diffusion coefficient value of gastric cancer by diffusion-weighted imaging: correlations with the histological differentiation and Lauren classification. Eur J Radiol 83:2122–2128

33. Ma L, Xu X, Zhang M et al (2017) Dynamic contrast-enhanced MRI of gastric cancer: correlations of the pharmacokinetic parameters with histological type, Lauren classification, and angiogenesis. Magn Reson Imaging 37:27–32